Materials and methods

Cell lines

MDCK cells were grown in DMEM (Thermo Fisher Scientific) supplemented with 10% fetal bovine serum (Sigma-Aldrich), HEPES buffer (Sigma-Aldrich), and 1 % penicillin/streptomycin in a humidified incubator at 37C with 5% CO2. To visualise the DNA during division, cells were transduced with lentivirus encoding H2B GFP (kind gift from Dr Susana Godinho, Barts Cancer Institute, Queen Mary University of London, UK). To visualise the localisation of cortical pulling forces on astral microtubules, we generated a stable cell line expressing LGN-GFP. For this, LGN-GFP was excised from a plasmid (pTK14, plasmid #37360, Addgene, USA) and inserted into a retroviral vector (pLPCX, Takara-Clontech, Japan). Retroviruses were then generated as previously described and transduced into wild-type MDCK cells. All cell lines were selected with appropriate antibiotics and sorted by flow cytometry before use. Cells were routinely tested for the presence of mycoplasma using the mycoALERT kit (Lonza, Switzerland).

Generating suspended MDCK monolayers

Suspended MDCK monolayers were made as described in (1). Briefly, a drop of collagen was placed between two test rods and left to dry at 37C to form a solid scaffold. The dry collagen was then rehydrated and cells were seeded on top of it and cultured for 48-72 hours until cells covered the whole of the collagen and part of each test rod. Immediately before each experiment, the collagen scaffold was removed via collagenase enzymatic digestion, leaving the monolayer of cells suspended between the two test rods (**Fig 1A**).

Imaging suspended MDCK monolayers

Tissues were imaged at 37C in a humidified atmosphere with 5% CO2. The imaging medium consisted of DMEM without phenol red supplemented with 10 % FBS. To visualize the shape of the cells during division, cell membranes were labelled with CellMask membrane stain for 10 min prior to collagen digestion following the manufacturer protocol (Thermo Fisher Scientific, UK). To visualise the boundaries of the suspended monolayer, AlexaFluor-647-conjugated dextran, 10,000MW (Thermo Fisher Scientific) was added at 20 μg ml^{-1} to the imaging medium.

XYZ stacks of the tissue before and after mechanical manipulation were obtained using a 40x objective (UPlanSApo, NA=1.25), on an Olympus IX83 inverted microscope equipped with a scanning laser confocal head (FV-1200, Olympus, Berlin, Germany). A single stack was obtained before, and the tissue was imaged for approximately 1h after the mechanical manipulation, acquiring stacks at intervals of 1-2 minutes with Z-slices spaced by 1 μm.

Mechanical manipulation of suspended MDCK monolayers

Mechanical manipulation of the MDCK monolayers along the X-axis was performed as previously described (2). A custom-made steel wire probe was connected to a 2D manual micromanipulator which was mounted onto a motorized platform (M-126.DG1 controlled through a C-863 controller, Physik Instrumente, Germany). The manual micromanipulator was used to position the probe so that it was wedged into a 'V'-shaped section of the stretching device arm, allowing both forward and backward movement to compress and stretch the monolayer (**Fig 1A**). The tissues were deformed by controlling the motion of the

motorized platform with a custom-written LabView program (National Instruments, USA). To ensure that the same part of the tissue was imaged before and after mechanical manipulation, the microscope stage (PS3J100, Prior Scientific Instruments, USA) was moved such that it matched the movement of the motorised platform using our LabView program to synchronise motion. In experiments, strain was applied at a 0.1%.s^{-1} strain rate, ensuring monolayers do not transiently buckle during application of compressive strain (3).

To apply cyclic stretch, our LabView programme generated sinusoidal displacement of the required amplitude and period.

Stress-strain relationships in suspended MDCK monolayers

To measure the evolution of strain applied at the tissue level, the entire width of the tissue was imaged with a 2x objective and bright field illumination at 1 second intervals on an inverted microscope with environmental control. To extract the strain exerted on the tissue from these videos, a script (Mathematica, Wolfram, USA) was written which used a Hough transform to detect the edges of the stretching device to which the tissue was attached. This data was used to compute the change in length of the tissue and the tissue strain.

Tissue-scale stress was varied by moving one of the test rods with the motorised micromanipulator (see **Fig 3A**). Then, tissue stress was measured as described in (3). Briefly, one extremity of the tissue was connected to a Nitinol wire which served as a force cantilever thanks its shape-memory properties. The force *F* exerted by the tissue was then deduced from the deflection *d* of the wire with respect to its reference position x_0: $d = x - x_0$ and $F = k.d,$ with *k* the stiffness of the wire and *x* the position of the wire. These positions were extracted from images of the monolayer acquired using a 2x objective (Olympus) mounted on an inverted microscope (Olympus IX-71) equipped with a CCD camera (GS3-U3-60QS7M-C, Pointgrey). To define the reference position of the wire x_0, tissues were detached from the device by cutting them with a tungsten needle at the end of the experiment. Stress was then defined as $\sigma = \frac{F}{w.h}$ with *w* the average width of the tissue and *h* the tissue thickness. Ramps of strain were applied at a strain rate of 0.1%.s^{-1}, a rate at which tissues exhibited a purely elastic behaviour with no viscous contribution (3). Tissue-scale strain was extracted as described above.

Quantification of cell strain during monolayer deformation

To measure strain at the cell level, MDCK cells labelled with CellMask membrane stain were imaged using a 60x oil immersion objective. A region of the monolayer, which contained both mitotic and interphase cells, was chosen close to the rigid arm of the stretching device. This region was maintained in the field of view of the camera during cyclic stretch and time-lapse imaging via manual movements in XY using the motorised microscope stage and refocusing. A custom-written script (Mathematica) used image cross-correlation to align the frames of the resulting videos and the Tissue Analyzer plugin of Image J was used to segment the cell shapes. Bounding boxes were fitted to each cell at each time point to calculate the temporal evolution of cell strain.

Quantification of cell shape and orientation in the XY-plane

By convention, the X-axis was taken as the axis of deformation and the Y-axis was perpendicular to that. The shape of mitotic and interphase cells was characterised from

confocal microscopy image stacks of monolayers stained with CellMask. The cell shape was manually marked using Fiji (http://fiji.sc/Fiji). The ellipse that best fitted the cell outline was calculated in Fiji; the length of the bounding box of the ellipse along the X-axis was taken as a measure of cell size along the X-axis, the width of the bounding box of the ellipse was taken as the cell size along the Y-axis, and the ellipse orientation was used as a measure of cell orientation. For each mitotic cell, the V-axis was taken along the midline of the metaphase plate and the U-axis along the spindle pole-to-pole axis. The UV plane is co-planar with the XY plane but rotated by an angle which defines the orientation of the spindle with respect to the direct of stretch (the X-angle). Measurements of cell height (cell size along the Z-axis) and cell length (along the U-axis) were obtained manually in Fiji from sectioning of the image stack along UZ planes. Cell shape and orientation were determined in the confocal image stack before and immediately after mechanical manipulation and additionally in the confocal image stack at the beginning of metaphase. Changes in cell height *h*, cell length *l*, and aspect ratio *h/l* were computed as $\delta l = {(l - l_0)}/{l_0}$, $\delta h = {(h - h_0)}/{h_0}$, and $\delta(\frac{h}{l}) = {\left(\frac{h}{l} - \frac{h_0}{l_0}\right)}/{(\frac{h_0}{l_0})}$.

Quantification of spindle orientation out-of-plane

Spindle orientation with respect to the Z-axis was determined at the beginning of metaphase, when the metaphase plate was formed, ($Z\text{-angle}_m$), and at the end of division, when closing of the cytokinetic furrow was complete, ($Z\text{-angle}_d$). The angles were measured from the cross-sections through the image stack along UZ planes. The metaphase spindle orientation ($Z\text{-angle}_m$) was measured as the angle between the line going through the metaphase plate and the line perpendicular to the monolayer plane (**Fig 1D, Fig S1A**). Spindle orientation at the end of division ($Z\text{-angle}_d$) was measured as the angle between the line going through the new junction between daughter cells and the line perpendicular to the monolayer plane (**Fig 1D**). In out-of-plane divisions, with high Z-angle, one daughter cell occasionally remained on top of the monolayer.

Quantification of metaphase plate height and spindle length

Spindle length and metaphase plate height were measured at the beginning of metaphase from the cross-sections through the image stack along UZ planes. To visualise the spindle, MDCK H2B GFP cells were incubated for 30 min before the start of imaging with the SiR-tubulin dye (Spirochrome, Switzerland). Spindle length was measured manually in Fiji as the distance between the two spindle pole bodies. Metaphase plate height was determined from the H2B GFP signal.

Quantification of cellular radii of curvature

Apical, basal and lateral mitotic cell outlines were manually marked from the CellMask signal at the beginning of metaphase in cross-sections through the image stack along XZ planes using Fiji. A circle was fitted through each of the marked outlines, and the respective radii were tabulated. Similarly, apical and basal outlines of interphase cells were manually marked from the CellMask signal and radii of curvature were determined in the same way as for the mitotic cells.

Quantification of apical contact angle

The apical contact angle, $\theta_{a,mi}$, between mitotic cells and their neighbours was measured at the beginning of metaphase from the CellMask signal in cross-sections through confocal image stacks along UZ planes using Fiji.

Drug treatments

To block Rho-kinase activity, monolayers were treated with Y-27632 (Tocris, UK) at a concentration of 50 µM, 10 minutes prior to imaging. To inhibit polymerisation of astral microtubules without significantly affecting the spindle, monolayers were treated with low doses of nocodazole (20 nM, Merckmillipore, UK) for 10mins before experiments. To increase myosin contractility, myosin phosphatases were inhibited by addition of 35 nM of calyculin A (Sigma-Aldrich, USA), 10 min before experiments. All drugs were dissolved in DMSO and were present throughout imaging.

Tubulin immunostaining

For immunostaining of microtubules, cells were fixed in ice-cold methanol at -20C before washing three times in PBS containing 10% horse serum (HS) for 5 min each. They were thenincubated with a mouse monoclonal primary antibody against α-tubulin (DMA1, 1:1000 dilution, Abcam, UK) for 1 hour at RT. This was followed by three washes in PBS+10%HS each lasting 5 min, incubation in goat anti-mouse secondary antibody conjugated with Alexa 488 (Thermofisher, 1:200 dilution) for 1 hour at RT, three washes in PBS+10%HS each lasting 5 min and staining of nucleic acids with Hoechst 33342 (5µg/mL-Merck Bio-sciences) for 5min. Following staining, cells were mounted in FluorSave reagent (Merckmillipore, UK) and imaged on an Olympus FV-1200 using a 100x objective (NA 1.40, Olympus, Germany).

Estimation of relative tension at subcellular surfaces

We use geometrical considerations to estimate the evolution of apical, lateral, and basal tensions from experimental measurements of the apical and basal radii of curvature at different tissue strains using Laplace's law.

Because Laplace's law assumes that surfaces can be approximated to portions of spheres, we first verified that monolayer profiles were similar when viewed along the axis of deformation (XZ profiles) and perpendicular to it (YZ profiles). To verify this, we measured the radii of curvature of interphase cells along profiles acquired in the XZ and YZ directions and found that these were not significantly different on either the apical or the basal side (**SI Appendix Fig S14D**). Based on these measurements, we concluded that cell apices and bases could be approximated to portions of a sphere.

According to Laplace's law, the radius of curvature is dictated by the interplay between the internal cellular pressure P and the surface tension $: r = \frac{2\gamma}{P}$. As apical and basal surfaces are exposed to the same internal pressure, the ratio of surface tensions can simply be inferred from the ratio of radii of curvature: $\frac{r_{apical}}{r_{basal}} = \frac{\gamma_{apical}}{\gamma_{basal}}$.

At the apical surface, we can use the Young-Dupré relationship to estimate the junctional tension $\gamma_{junctional}$ from γ_{apical}:

$$\gamma_{junctional} = 2\gamma_{apical}.\cos(\theta_a/_2)$$

with θ_a the apical angle of contact. If we approximate the apical side of the monolayer to a series of portions of circle with the same radius of curvature r_{apical} and assume that all cells have a width a, θ_a can be estimated as:

$$\theta_a = \pi - 2\ sin^{-1}(\frac{a}{r_{apical}})$$

By combining the two equations, we obtain:

$$\frac{\gamma_{junctional}}{\gamma_{apical}} = \frac{a}{r_{apical}}$$

Similar relationships can also be written for the relationship between junctional and basal tensions. In this study, we normalise surface tensions to γ_{basal} because our previous work has shown that tension in the basal surfaces is highest (4).

Therefore, by measuring a, r_{apical}, and r_{basal} as a function of applied strain or chemical treatment, we can determine how surface tensions vary with respect to one another with strain or chemical treatment.

Computational modelling

To mimic experimental testing of suspended monolayers, we use a finite element model implemented in Julia (MIT, USA). In this model, the tissue is discretised as a triangular mesh where each cell is represented by a hexagon consisting of six triangles (**SI Appendix Fig S11**). Each triangle side is modelled as a spring with spring constant k, length l, and rest length l_0. The mechanical connection between springs is modelled with pins that allow free rotation around the extremities of each bar.

We assumed that the stress-free shape of the monolayer was a rectangle of 20 x 20 hexagonal cells. To simulate myosin contractility within each cell, we imposed an initial prestress γ in each spring by setting the rest length l_0 such that $\gamma = k(l_{init} - l_0)$, where l_{init} is the length in the reference configuration (0% strain). To mimic the presence of mitotic cells within the monolayer, we modified the stiffness k and the contractility γ of one hexagon within the centre of the monolayer such they were 2.5-fold and 2-fold larger, respectively, to match the stiffer spring constant and greater contractility observed in mitotic cells (blue elements, **SI Appendix Fig S11**, **Fig 4B**).

Displacement boundary conditions were imposed to nodes on each of the vertical edges of monolayer to allow simulation of uniaxial deformation and the horizontal edges were left free (**SI Appendix Fig S11**). To simulate compressive/tensile loading, displacements d were imposed along the horizontal axis (X-axis). To identify the equilibrium configuration, we used the finite element method (5).

From the displacements of each node, we can compute the stress tensor acting on any subarea A as

$$\sigma = \frac{1}{A}\sum_{i=1}^{N} \sigma_i \begin{bmatrix}(l_i)_x \\ (l_i)_y\end{bmatrix} [(l_i)_x \quad (l_i)_y]$$

where N is the number of elements within the sub-area, σ_i is the stress along element i, and l_x and l_y are the length of element i projected along the x- and y-axis, respectively.

The model is first used to assess the stress at different cell locations assuming no mitotic cells are present. By comparing the principal stresses along the X- and Y-directions close to the centre of the monolayer to those occurring further away from the centre (thus comparing the stress tensors in columns 2 vs 4 and 3 vs 5 in **SI Appendix Fig S12**), we conclude that the stress tensors within the monolayer are approximately homogeneous, consistent with the experimental observation of homogeneous strain in stretched monolayers (6). Therefore, the stress on the test rods measured in experiments is a good approximation of the stress experienced by cells in the centre of the monolayer. A similar conclusion was reached when a dividing cell is present in the centre of the monolayer (**SI Appendix Fig S13**).

Simulation	**Spring constant k**	**Strain**	**Contractility γ**
Control – Untreated monolayer	1	0	0.35
Compressed untreated monolayer	1	-30%	0.35
Compressed monolayer with increased contractility	1.5	-30%	0.5
Monolayer with reduced contractility	0.7	0	0.1
Stretched monolayer with reduced contractility	0.7	50%	0.1

Table 1: Model parameters for simulation of different experimental conditions displayed in **Appendix Fig S12, S13**.

Statistical and data analysis

All other data and most statistical analysis was performed in MATLAB R2018a (Mathworks, Natick, MA, USA).

Boxplots show the median value (red line), the first and third quartile (bounding box) and the whiskers extend to the most extreme data points that are not outliers. Outliers were defined as being either larger than Q3+1.5*IQR or smaller than Q1-1.5*IQR, with Q1 the value of the first quartile, Q3 the value of the third quartile, and IQR=Q3-Q1. Raw data points are plotted on top of all boxplots. All tests of statistical significance are Wilcoxon rank-sum tests unless otherwise stated. In statistical comparisons of populations with the Wilcoxon rank-sum test, we included outliers because this statistical test is robust to their presence.

Fisher exact tests were used to assess the change in the proportion of cells dividing in plane in response to a treatment. For this, we categorised dividing cells as having low Z-angles (<30°, in-plane) or high Z-angles (≥30°, out-of-plane). We then computed the Fisher exact test statistics using SPSS (IBM, Armonk, NY, USA).

To compare populations to a constant, we used a two-tailed z-test implemented in Excel (Microsoft, Redmond, WA, USA).

All correlation coefficients were calculated using the CORREL function in Excel. The p-value was calculated as the corresponding two-sided p-value for the t-distribution with *(n-2)* degrees of freedom, where $t = \sqrt{n-2}/\sqrt{(1-r^2)}$, and n equals sample size.

For all statistical tests, we considered a threshold of 0.01 for statistical significance. We denoted p values <0.01 with '*' and p values <0.001 with '**'.

Image processing

Image processing was performed with Fiji.

References

1. A. R. Harris, *et al.*, Generating suspended cell monolayers for mechanobiological studies. *Nature Protocols* **8**, 2516–2530 (2013).

2. T. P. J. Wyatt, *et al.*, Emergence of homeostatic epithelial packing and stress dissipation through divisions oriented along the long cell axis. *Proceedings of the National Academy of Sciences* **112**, 5726–5731 (2015).

3. T. P. J. Wyatt, *et al.*, Actomyosin controls planarity and folding of epithelia in response to compression. *Nat. Mater.* **19**, 109–117 (2020).

4. J. Fouchard, *et al.*, Curling of epithelial monolayers reveals coupling between active bending and tissue tension. *Proceedings of the National Academy of Sciences* **117**, 9377–9383 (2020).

5. J. N. Reddy, *Introduction to the finite element method* (McGraw-Hill Education, 2019).

6. A. R. Harris, *et al.*, Characterizing the mechanics of cultured cell monolayers. *Proceedings of the National Academy of Sciences* **109**, 16449–16454 (2012).

Supplementary Figures

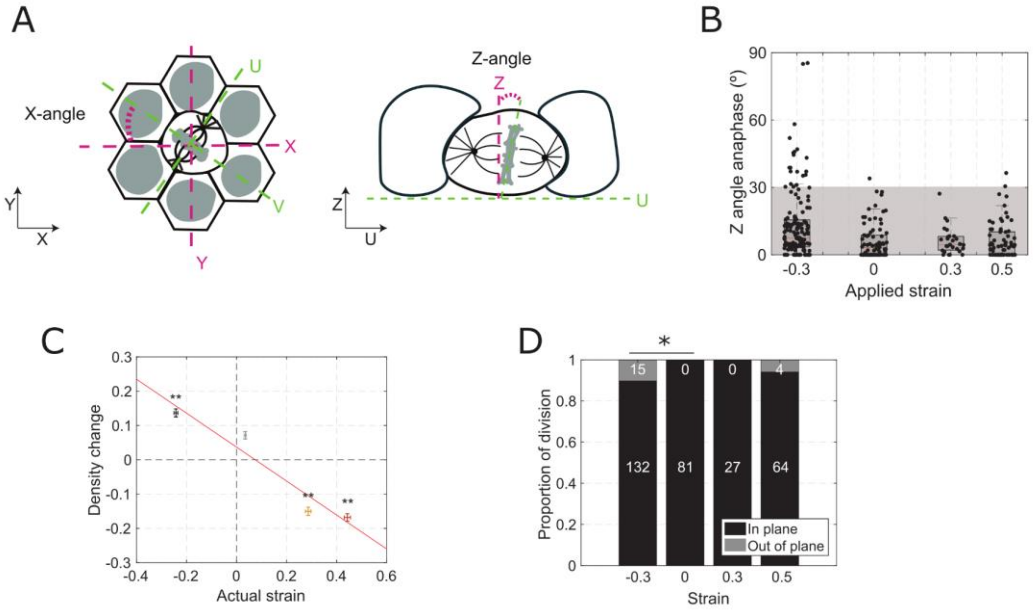

Figure S1. Characterisation of Z-angle, density change and out-of-plane division in response to mechanical manipulation.

- **A.** Left: Diagram depicting the definition of the X-angle. For each dividing cell, a cell-centered UV referential was defined with the U-axis oriented along the pole-to-pole axis and the V-axis oriented along the midline of the metaphase plate. The smallest angle between the V-axis and the X-axis was defined as the X-angle.
  Right: Diagram depicting the definition of the Z-angle. A UZ profile is generated and the axis bisecting the metaphase plate is determined (green dashed line). The Z-angle is defined as the smallest angle between the Z-axis and the axis of the metaphase plate.
- **B.** Distribution of the spindle Z-angle at the end of division for different applied strains in control monolayers. Box plots indicate the 25th and 75th percentiles, the red line indicates the median, and the whiskers extend to the most extreme data points that are not outliers. Individual data points are indicated by black dots. Greyed region highlights Z-angles < 30°. The number of cells examined for each condition was N=156 for -30% strain, N=80 for 0% strain, N=27 for 30% strain, and N=69 for 50% strain. Experiments were performed on n=14, n=8, n=4, and n=8 independent days, respectively.
- **C.** Change in density for different applied deformations. Cell density and actual strain were computed from images of the monolayer before and after deformation for target strains of -30%, 0%, 30%, and 50% respectively. Horizontal and vertical whiskers indicate the standard error of the mean. Change in density was computed relative to the 0% strain condition. Density changes for different target strains were compared using a WRST. The p-value was $p=1.4\ 10^{-8}$ for -30% strain vs 0% strain, $p=3.3\ 10^{-14}$ for 30% strain vs 0% strain, and $p=3.4\ 10^{-14}$ for 50% strain vs 0% strain. The number of cells examined for each condition was N=113 for -30% strain, N=66 for 0% strain, N=27 for 30% strain and N=71 for 50% strain. Experiments were from at least 3 independent days.
- **D.** Proportion of spindles dividing in-plane and out-of-plane as a function of applied strain. Out-of-plane divisions are shown in dark grey and in-plane divisions in black. The number of divisions in each category is indicated in the corresponding region of the bar. Distributions were compared to 0% strain with a Fisher Exact test. The p-values were $p<0.01$ for -30% compressive strain, $p=1$ for 30% strain, and $p=0.04$ for 50% strain.

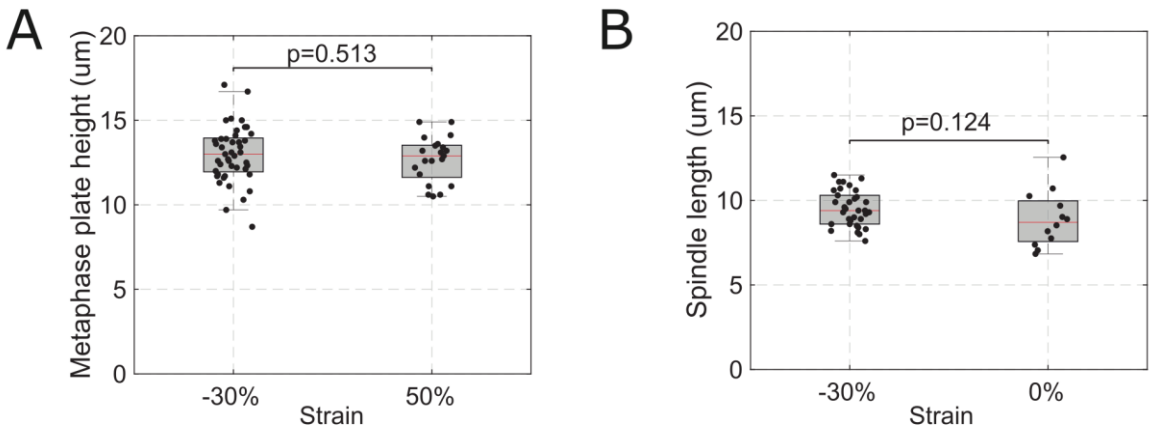

Figure S2. Characterisation of spindle length and metaphase plate height. Box plots indicate the 25th and 75th percentiles, the red line indicates the median, and the whiskers extend to the most extreme data points that are not outliers. Individual data points are indicated by black dots.

A. Metaphase plate height in cells in compressed and stretched monolayers. N=45 for -30% strain and N=21 for 50% strain, p=0.513 (WRST).

B. Spindle length for metaphase cells in control and compressed monolayers. N=12 for 0% strain and N=34 for -30% strain, p=0.124 (WRST).

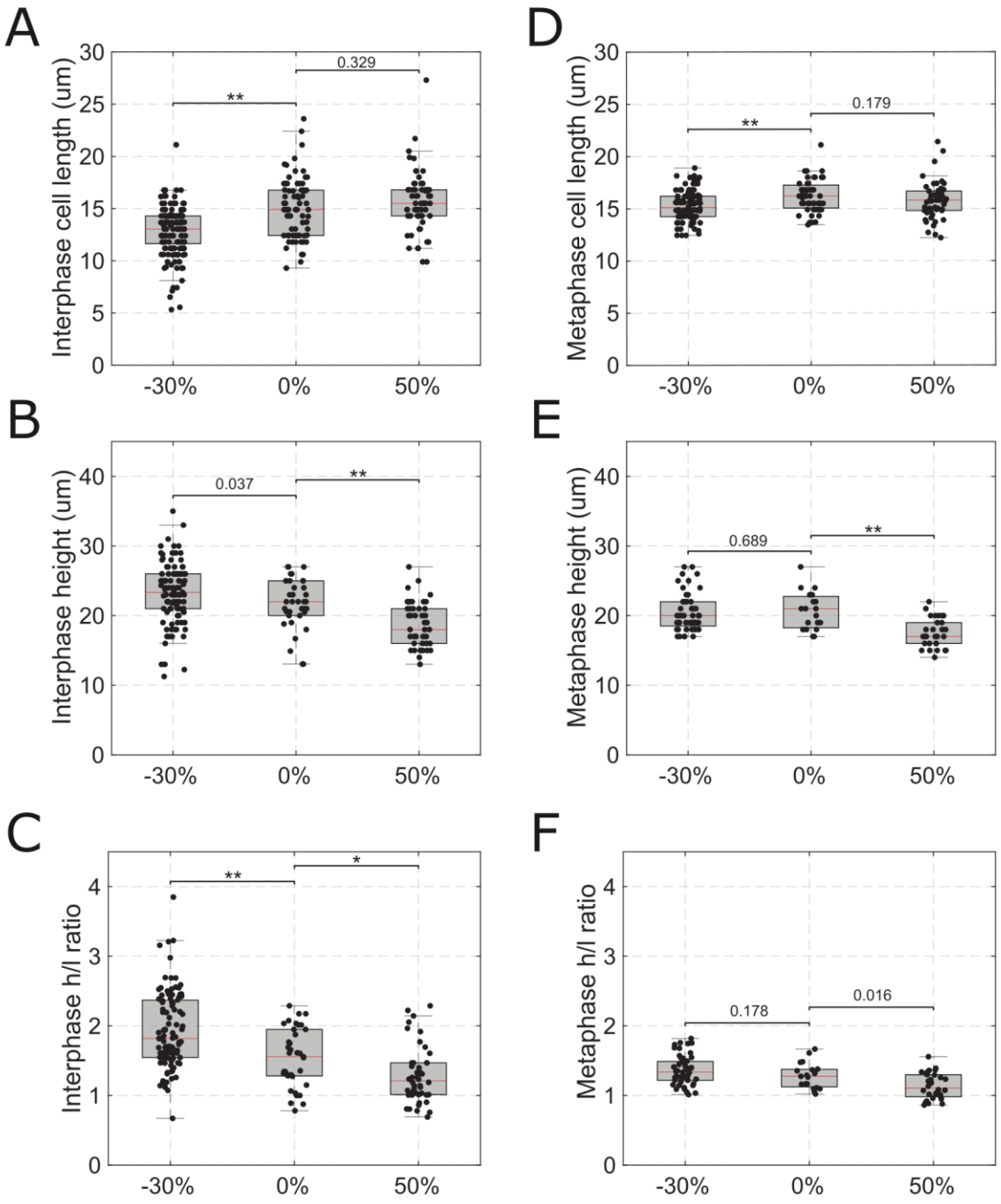

Figure S3: Changes in cell size, height and aspect ratio in interphase cells and metaphase cells in response to deformation. Box plots indicate the 25th and 75th percentiles, the red line indicates the median, and the whiskers extend to the most extreme data points that are not outliers. Individual data points are indicated by black dots.

A. Interphase cell length as a function of strain. N=149 cells for -30% strain, N=76 cells for 0% strain, and N=67 cells for 50% strain. -30% strain vs 0% strain: $p=2.4\ 10^{-8}$, 0% strain vs +50% strain: p=0.329 (WRST).

B. Interphase cell height as a function of strain. N=107 cells for -30% strain, N=37 cells for 0% strain, and N=46 cells for 50% strain. -30% strain vs 0% strain: p=0.037, 0% strain vs +50% strain: p=0.0005 (WRST).

C. Interphase cell aspect ratio as a function of strain. N=107 cells for -30% strain, N=37 cells for 0% strain, and N=46 cells for 50% strain. -30% strain vs 0% strain: p=0.0003, 0% strain vs +50% strain: p=0.009 (WRST).
D. Metaphase cell height as a function of strain. N=114 cells for -30% strain, N=55 cells for 0% strain, and N=54 cells for 50% strain. 0% strain vs -30% strain: p=0.0004, 0% strain vs 50% strain: p=0.179 (WRST).
E. Metaphase cell length as a function of strain. N=52 cells for -30% strain, N=19 cells for 0% strain, and N=31 cells for 50% strain. 0% strain vs -30% strain: p=0.689, 0% strain vs 50% strain: p=0.0001 (WRST).
F. Metaphase cell aspect ratio as a function of strain. N=52 cells for -30% strain, N=19 cells for 0% strain, and N=30 cells for 50% strain. 0% strain vs -30% strain: p=0.178, 0% strain vs 50% strain: p=0.016 (WRST).

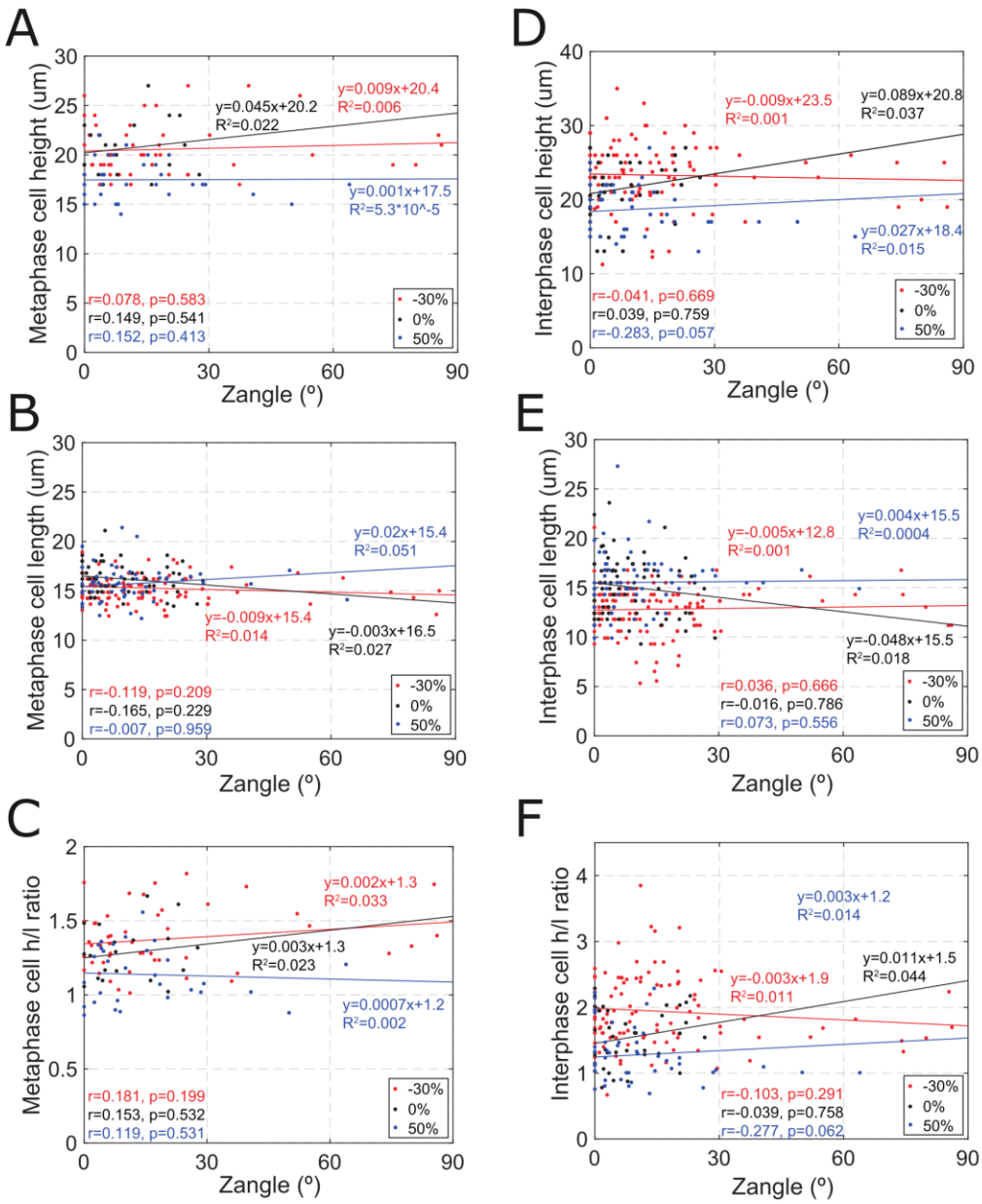

Figure S4. Spindle Z-angle is not correlated with the length, height, or aspect ratio of metaphase or interphase cells. The slope of the linear regression, the coefficient of determination R^2, the correlation coefficient r, and the p-value for each strain are indicated on each graph.

A. Spindle Z-angle as a function of cell height for cells in metaphase subjected to -30% strain (red), 0% strain (black), and 50% strain (blue).

-30%: Correlation coefficient, r = 0.078, p-value (two-tailed Student's t-distribution) = 0.583.
0%: Correlation coefficient, r = 0.149, p-value (two-tailed Student's t-distribution) = 0.541.
50%: Correlation coefficient, r = -0.152, p-value (two-tailed Student's t-distribution) = 0.413.

B. Spindle Z-angle as a function of cell length for cells in metaphase subjected to -30% strain (red), 0% strain (black), and 50% strain (blue).

-30%: Correlation coefficient, r = -0.119, p-value (two-tailed Student's t-distribution) = 0.209.
0%: Correlation coefficient, r = -0.165, p-value (two-tailed Student's t-distribution) = 0.229.
50%: Correlation coefficient, r = -0.007, p-value (two-tailed Student's t-distribution) = 0.959.

C. Spindle Z-angle as a function of cell h/l ratio for cells in metaphase subjected to -30% strain (red), 0% strain (black), and 50% strain (blue).
-30%: Correlation coefficient, r = 0.181, p-value (two-tailed Student's t-distribution) = 0.199.
0%: Correlation coefficient, r = 0.153, p-value (two-tailed Student's t-distribution) = 0.532.
50%: Correlation coefficient, r = 0.119, p-value (two-tailed Student's t-distribution) = 0.531.

D. Spindle Z-angle as a function of cell height measured in interphase for cells that go on to divide. Monolayers were subjected to -30% strain (red), 0% strain (black), and 50% strain (blue).
-30%: Correlation coefficient, r = -0.041, p-value (two-tailed Student's t-distribution) = 0.669.
0%: Correlation coefficient, r = 0.039, p-value (two-tailed Student's t-distribution) = 0.759.
50%: Correlation coefficient, r = -0.283, p-value (two-tailed Student's t-distribution) = 0.057.

E. Spindle Z-angle as a function of cell length measured in interphase for cells that go on to divide. Monolayers were subjected to -30% strain (red), 0% strain (black), and 50% strain (blue).
-30%: Correlation coefficient, r = 0.036, p-value (two-tailed Student's t-distribution) = 0.666.
0%: Correlation coefficient, r = -0.016, p-value (two-tailed Student's t-distribution) = 0.786.
50%: Correlation coefficient, r = 0.073, p-value (two-tailed Student's t-distribution) = 0.556.

F. Spindle Z-angle as a function of cell h/l ratio measured in interphase for cells that go on to divide. Monolayers were subjected to -30% strain (red), 0% strain (black), and 50% strain (blue).
-30%: Correlation coefficient, r = -0.103, p-value (two-tailed Student's t-distribution) = 0.291.
0%: Correlation coefficient, r = -0.039, p-value (two-tailed Student's t-distribution) = 0.758.
50%: Correlation coefficient, r = -0.277, p-value (two-tailed Student's t-distribution) = 0.062.

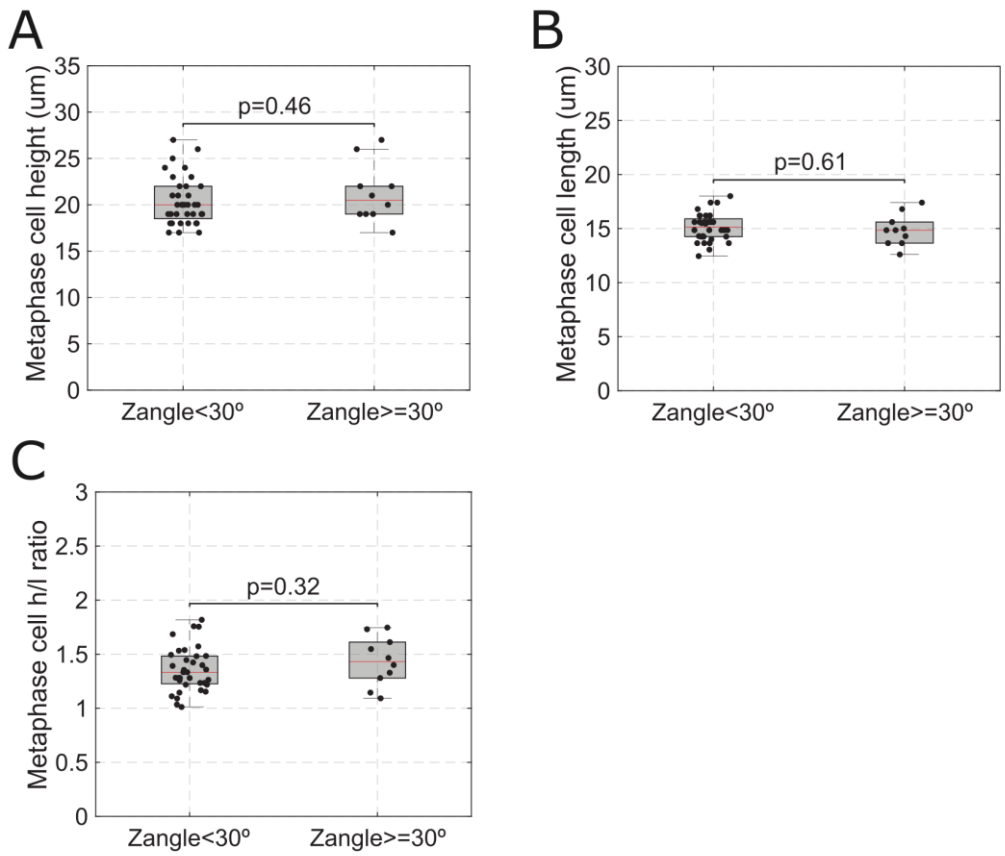

Figure S5. Cell dimensions and shape are not different for divisions with low and high Z-angles. Box plots indicate the 25th and 75th percentiles, the red line indicates the median, and the whiskers extend to the most extreme data points that are not outliers. Individual data points are indicated by black dots.

- **A.** Cell height at metaphase as a function of spindle Z-angle for dividing cells in compressed monolayers (-30 %). Metaphase spindle Z-angles were categorised as either in-plane (Z-angle<30°), or out-of-plane (Z-angle≥ 30°). Comparison with a WRST: p=0.46. N=35 cells for Z-angle<30° and N=10 for Z-angle≥ 30°.
- **B.** Cell length at metaphase as a function of spindle Z-angle for dividing cells in compressed monolayers (-30 %). Metaphase spindle Z-angles were categorised as either in-plane (Z-angle<30°), or out-of-plane (Z-angle≥ 30°). Comparison with a WRST: p=0.61. N=35 cells for Z-angle<30° and N=10 for Z-angle≥ 30°.
- **C.** Ratio of cell height/length at metaphase as a function of spindle Z-angle for dividing cells in compressed monolayers (-30 %). Metaphase spindle Z-angles were categorised as either in-plane (Z-angle<30°), or out-of-plane (Z-angle≥ 30°). Data as in Fig 2D. Comparison with a WRST: p=0.32. N=35 cells for Z-angle<30° and N=10 for Z-angle≥ 30°.

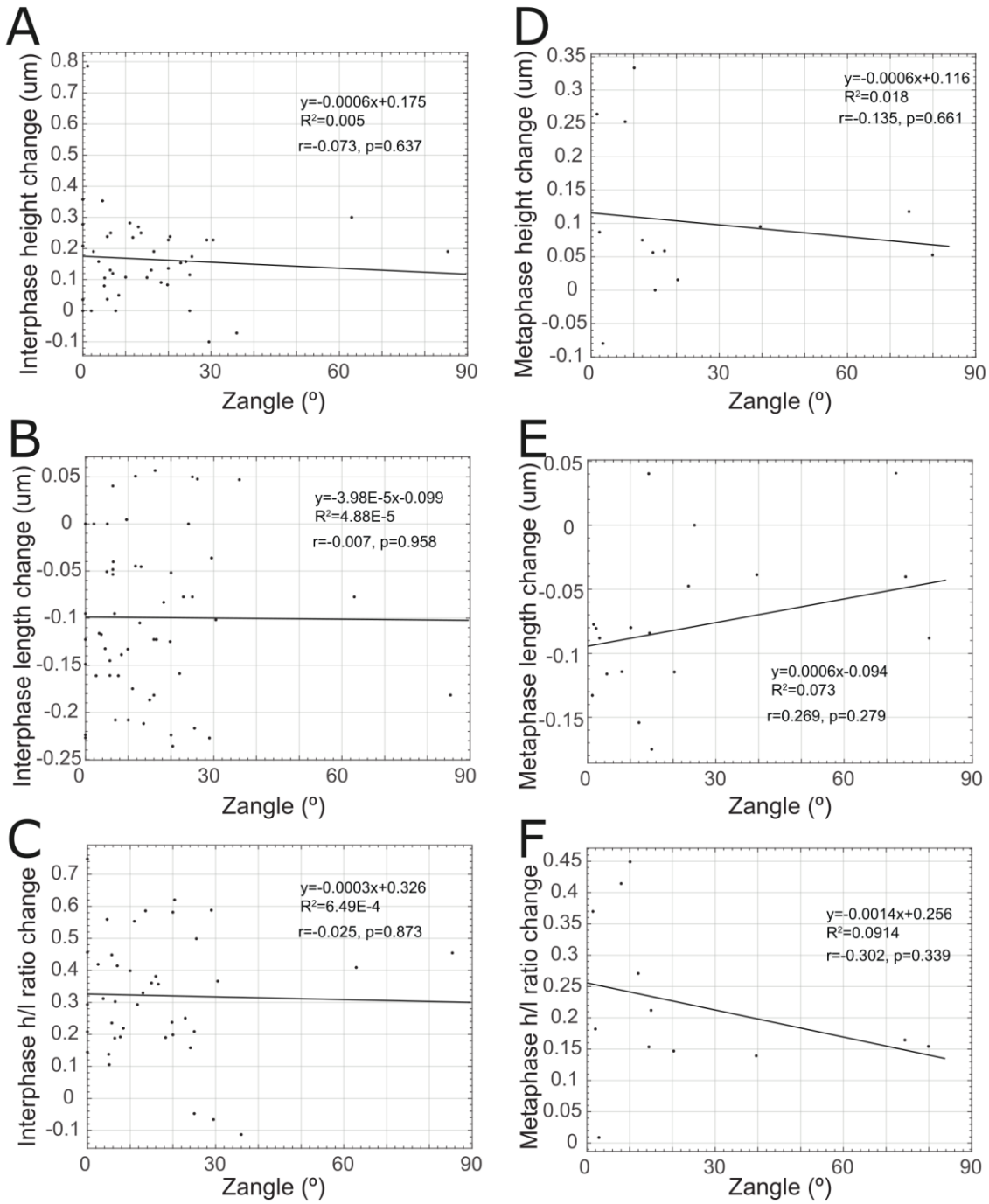

Figure S6: Spindle Z-angle is not correlated with changes in length, height, or aspect ratio of metaphase or interphase cells. The slope of the linear regression, the coefficient of determination R^2, the correlation coefficient r, and the p-value are indicated on each graph for -30% strain.

- **A.** Spindle Z-angle as a function of change in cell height δh for cells in interphase that go on to divide after being subjected to -30% strain. Correlation coefficient, r = 0.073, p-value (two-tailed Student's t-distribution) = 0.637.
- **B.** Spindle Z-angle as a function of change in cell length δl for cells in interphase that go on to divide after being subjected to -30% strain. Correlation coefficient, r = 0.007, p-value (two-tailed Student's t-distribution) = 0.958.
- **C.** Spindle Z-angle as a function of change in h/l ratio for cells in interphase that go on to divide

after being subjected to -30% strain. Correlation coefficient, r = -0.025, p-value (two-tailed Student's t-distribution) = 0.873.

D. Spindle Z-angle as a function of change in cell height δh measured in metaphase for cells subjected to -30% strain. 30%: Correlation coefficient, r = -0.135, p-value (two-tailed Student's t-distribution) = 0.661.

E. Spindle Z-angle as a function of change in cell length δl measured in metaphase subjected to -30% strain. Correlation coefficient, r = 0.269, p-value (two-tailed Student's t-distribution) = 0.279.

F. Spindle Z-angle as a function of change in cell h/l ratio measured in metaphase for cells subjected to -30% strain. Correlation coefficient, r = -0.302, p-value (two-tailed Student's t-distribution) = 0.339.

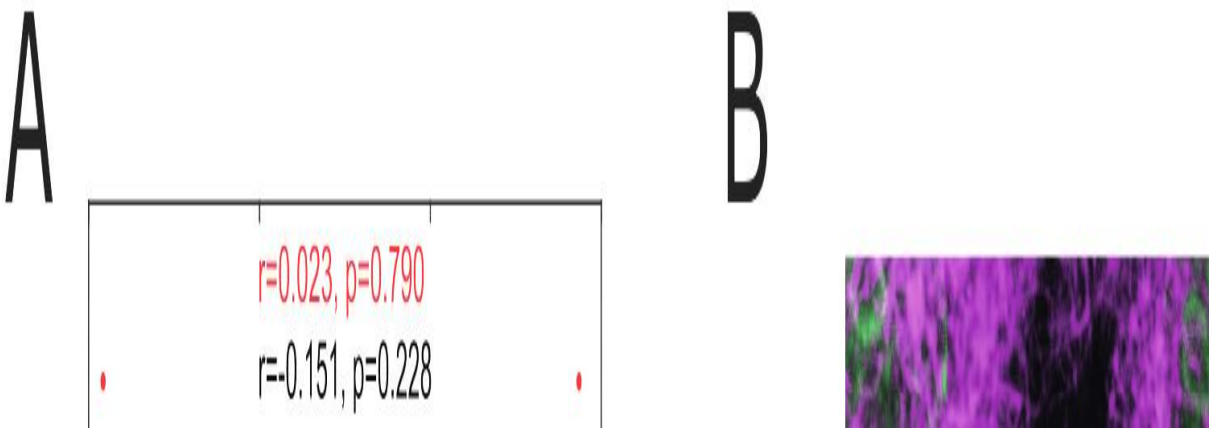

Figure S7 Spindle Z-angle does not correlate with density change and treatment with nocodazole disrupts astral microtubules.

A. Spindle Z-angle as a function of density change for cells in monolayers subjected to -30% strain (red), 0% strain (black), 30% strain (green), 50% strain (blue). The slope of the regression, the coefficient of determination R^2, the correlation coefficient r, and the p-value for each strain are indicated on the graph. N=128 cells for -30% strain, N=65 cells for 0% strain, N=27 cells for 30% strain, and N=62 cells for 50% strain.

-30%: Correlation coefficient, r = 0.023, p-value (two-tailed Student's t-distribution) = 0.790.
0%: Correlation coefficient, r = -0.151, p-value (two-tailed Student's t-distribution) = 0.228.
30%: Correlation coefficient, r = 0.153, p-value (two-tailed Student's t-distribution) = 0.445.
50%: Correlation coefficient, r = 0.027, p-value (two-tailed Student's t-distribution) = 0.835.

B. Representative immunofluorescence images of WT MDCK cells stained for α-tubulin. Cells were treated with DMSO (control) or with 20nM nocodazole to disrupt astral microtubules. Yellow arrows indicate astral microtubules. DNA is stained with DAPI and shown in green, tubulin staining is shown in magenta. Scale bar: 10μm.

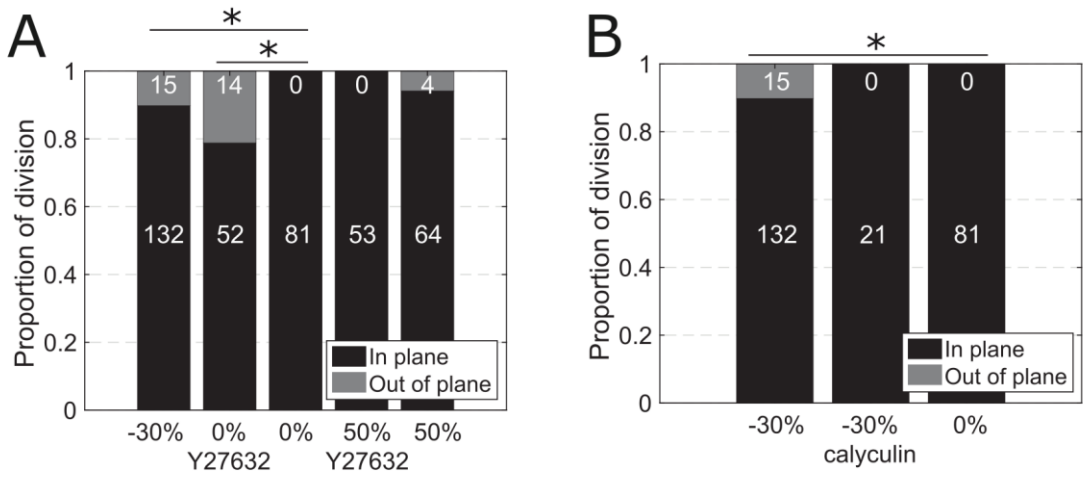

Figure S8: Out-of-plane division is induced by low tension and can be rescued by orthogonal treatments increasing tissue tension.

A. Proportion of spindles dividing in-plane and out-of-plane as a function of strain and drug treatment. Out-of-plane divisions are shown in grey and in-plane divisions in black. The number of divisions in each category is indicated in the corresponding region of the bar. Comparison of the distributions to 0% strain with a Fisher Exact test. The p-values were $p<0.01$ for -30% compressive strain, $p<0.01$ for 0% with Y27632, $p=1$ for 50% strain with Y27632, and $p=0.04$ for 50% strain. Data from Fig 1E and Fig 3E.

B. Proportion of spindles dividing in-plane and out-of-plane as a function of strain and drug treatment. Out-of-plane divisions are shown in in grey and in-plane divisions in black. The number of divisions in each category is indicated in the corresponding region of the bar. Comparison of the distributions to 0% strain with a Fisher Exact test. The p-values were $p<0.01$ for -30% compressive strain, and $p=1$ for -30% strain with calyculin. Data from Fig 1E and Fig 3F.

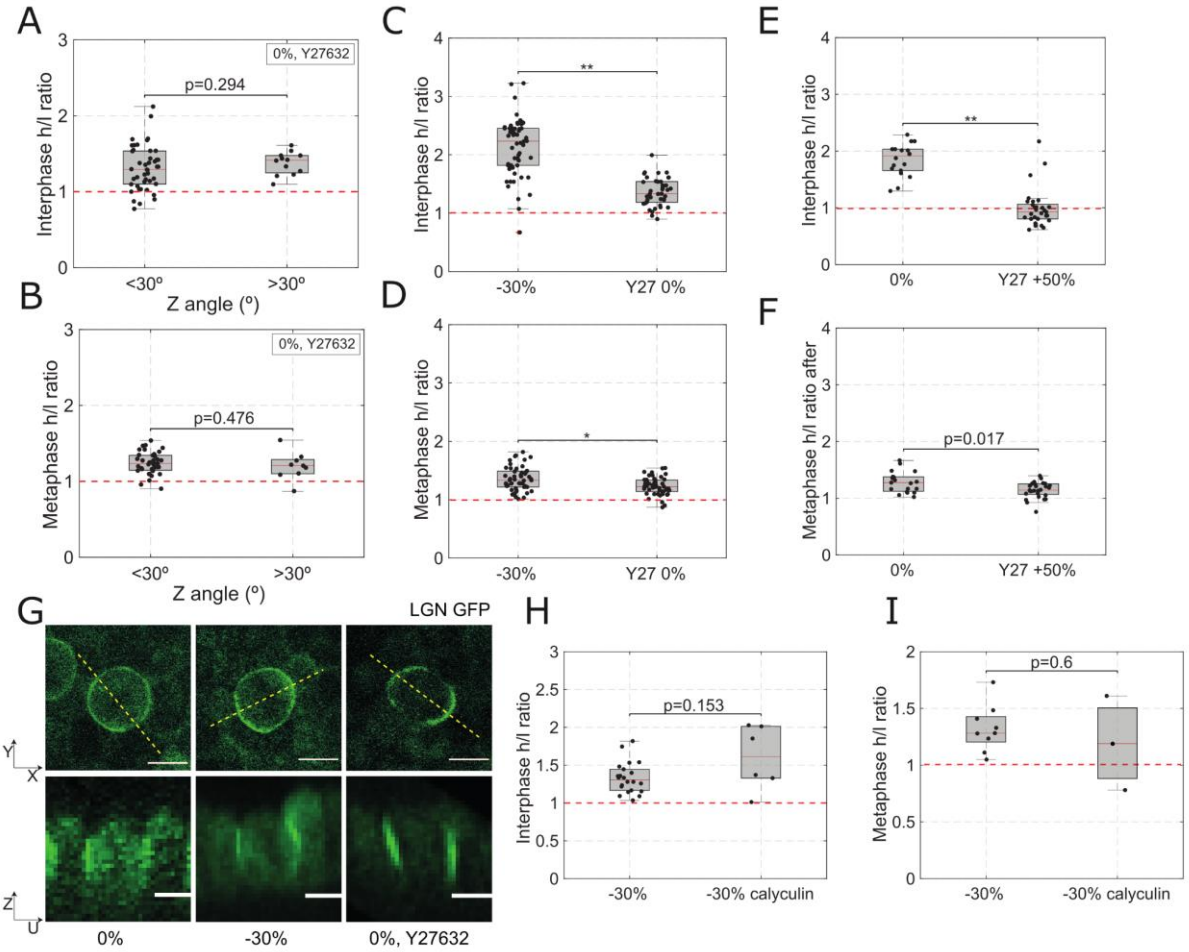

Figure S9. Cell shape and the localisation of spindle positioning proteins do not correlate with poor in-plane orientation in response to Y27632 treatment.

(A-F, H-I) Box plots indicate the 25th and 75th percentiles, the red line indicates the median, and the whiskers extend to the most extreme data points that are not outliers. Individual data points are indicated by black dots.

- **A.** Height/length ratio of interphase cells in monolayers subjected to 0% strain and treated with Y27632 as a function of metaphase Z-angle for cells that go on to divide. Metaphase spindle Z-angles were categorised as either in-plane (Z-angle<30°), or out-of-plane (Z-angle≥30°). Data from Fig 3E. N=44 cells for <30% condition, N=12 cells for >30% condition.
- **B.** Height/length ratio of metaphase cells in monolayers subjected to 0% strain and treated with Y27632 as a function of metaphase Z-angle for cells that go on to divide. Metaphase spindle Z-angles were categorised as either in-plane (Z-angle<30°), or out-of-plane (Z-angle≥30°). Data from Fig 3E. N=39 cells for <30% condition, N=9 cells for >30% condition.
- **C.** Height/length ratio of interphase cells in monolayers subjected to 30% compressive strain or to 0% strain and treated with Y27632. WRST, $p = 1x10^{-11}$. Data from Fig 1E and Fig 3E. N=57 cells for 30% condition, N=41 cells for 0%, Y27632 condition.
- **D.** Height/length ratio of metaphase cells in monolayers subjected to 30% compressive strain or to 0% strain and treated with Y27632. WRST, p = 0.002. Data from Fig 1E and Fig 3E. N=52 cells for 30% condition, N=48 cells for 0%, Y27632 condition.
- **E.** Height/length ratio of interphase cells in monolayers at 0% strain or treated with Y27632 and subjected to 50% strain. WRST, $p = 3x10^{-7}$. Data from Fig 1E and Fig 3E. N=18 cells for 0% condition, N=29 cells for 50%, Y27632 condition.

F. Height/length ratio of metaphase cells in monolayers at 0% strain or treated with Y27632 and subjected to 50% strain. WRST: p = 0.017. Data from Fig 1E and Fig 3E. N=18 cells for 0% condition, N=29 cells for 50%, Y27632 condition.

G. Representative localisation of LGN in dividing cells in a monolayer subjected to 0% strain, -30% compressive strain, and 0% strain with Y27632 treatment viewed in the XY (top) and UZ (bottom) planes. Dashed yellow lines indicate the locations at which UZ profiles were taken. Scale bars: 10 μm.

H. Height/length ratio of interphase cells in monolayers subjected to -30% compressive strain, with and without calyculin treatment. WRST, p = 0.15. Data from Fig 3F. N=22 cells for -30% condition, N=6 cells for -30%, calyculin condition.

I. Height/length ratio of metaphase cells in monolayers subjected to -30% compressive strain, with and without calyculin treatment. WRST, p = 0.6. Data from Fig 3F. N=9 cells for -30% condition, N=3 cells for -30%, calyculin condition.

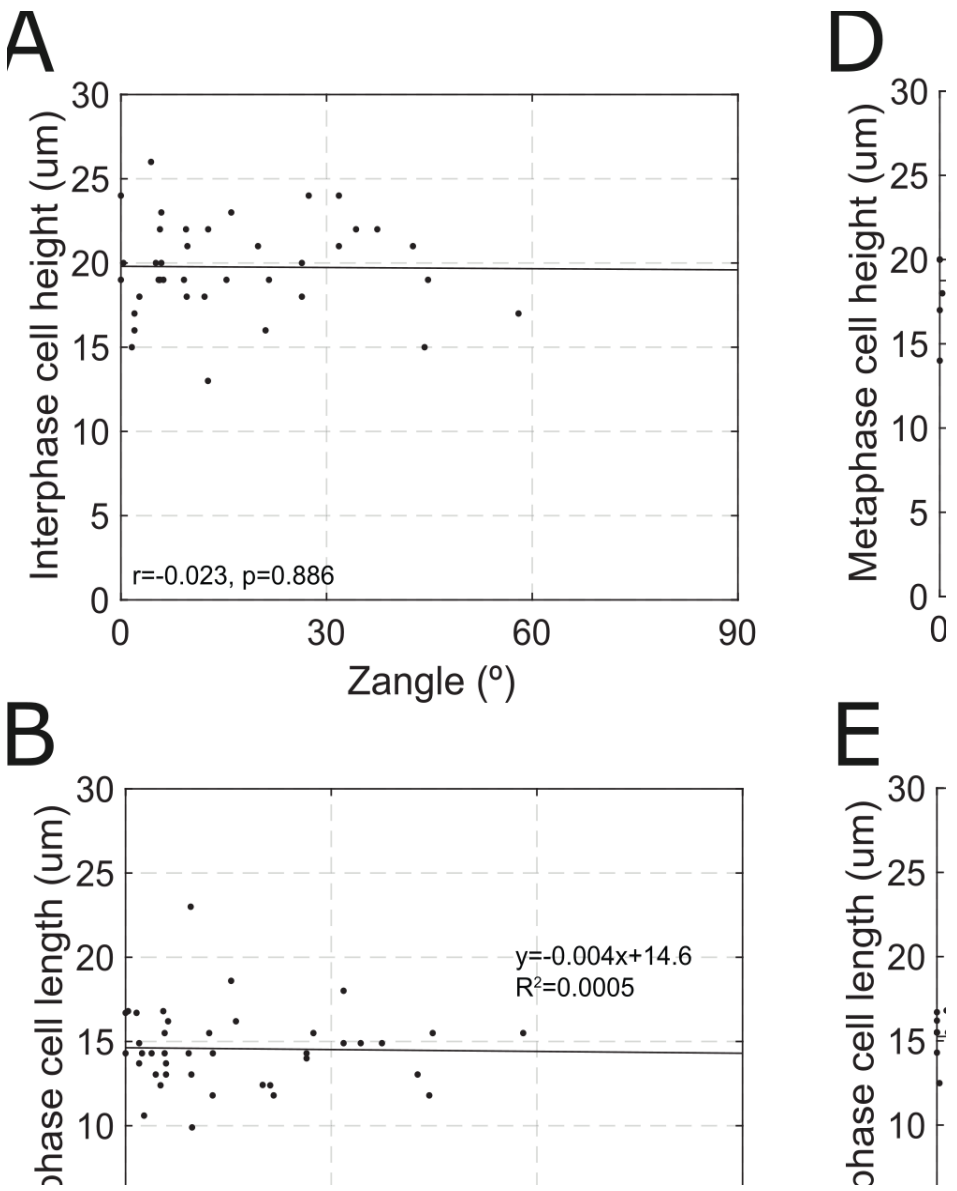

Figure S10. Cell height, length and shape do not correlate with Z-angle for cells treated with Y27632.

The slope of the linear regression, the coefficient of determination R^2, the correlation coefficient r, and the p-value are indicated on each graph.

- **A.** Spindle Z-angle as a function of cell height for cells in interphase subjected to Y27632 treatment and that go on to divide.
  Correlation coefficient, r = -0.023, p-value (two-tailed Student's t-distribution) = 0.886.
- **B.** Spindle Z-angle as a function of cell length for cells in interphase subjected to Y27632 treatment and that go on to divide.
  Correlation coefficient, r = -0.012, p-value (two-tailed Student's t-distribution) = 0.939.
- **C.** Spindle Z-angle as a function of cell h/l ratio for cells in interphase subjected to Y27632 treatment and that go on to divide.
  Correlation coefficient, r = -0.031, p-value (two-tailed Student's t-distribution) = 0.852.
- **D.** Spindle Z-angle as a function of cell height for cells in metaphase subjected to Y27632 treatment.
  Correlation coefficient, r = -0.239, p-value (two-tailed Student's t-distribution) = 0.136.

E. Spindle Z-angle as a function of cell length for cells in metaphase subjected to Y27632 treatment.
Correlation coefficient, r = -0.103, p-value (two-tailed Student's t-distribution) = 0.526.

F. Spindle Z-angle as a function of cell h/l ratio for cells in metaphase subjected to Y27632 treatment.
Correlation coefficient, r = -0.146, p-value (two-tailed Student's t-distribution) = 0.369.

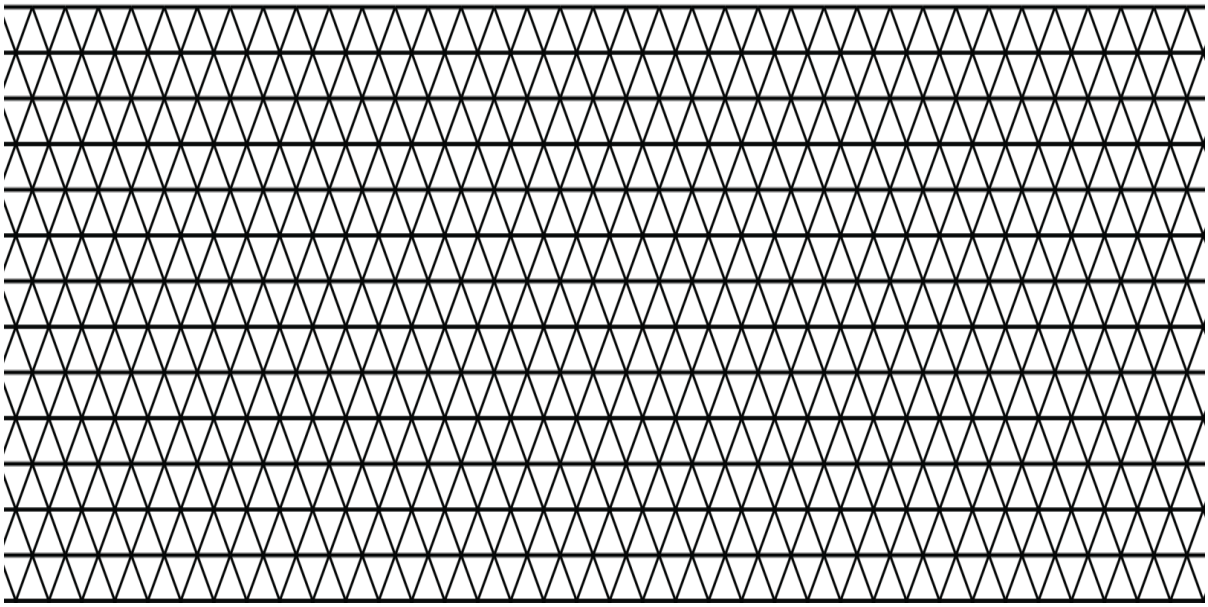

Figure S11. Sketch of the 2D planar monolayer model. The epithelial monolayer is discretised into triangles and subjected to displacement boundary conditions at its vertical edges while the horizontal edges are left free. Each triangle edge consists of a linear elastic element. The blue elements at the centre of the structure exemplify a mitotic cell (i.e. the stiffness and contractility of these structural elements are consistently increased to simulate the presence of a dividing cell).

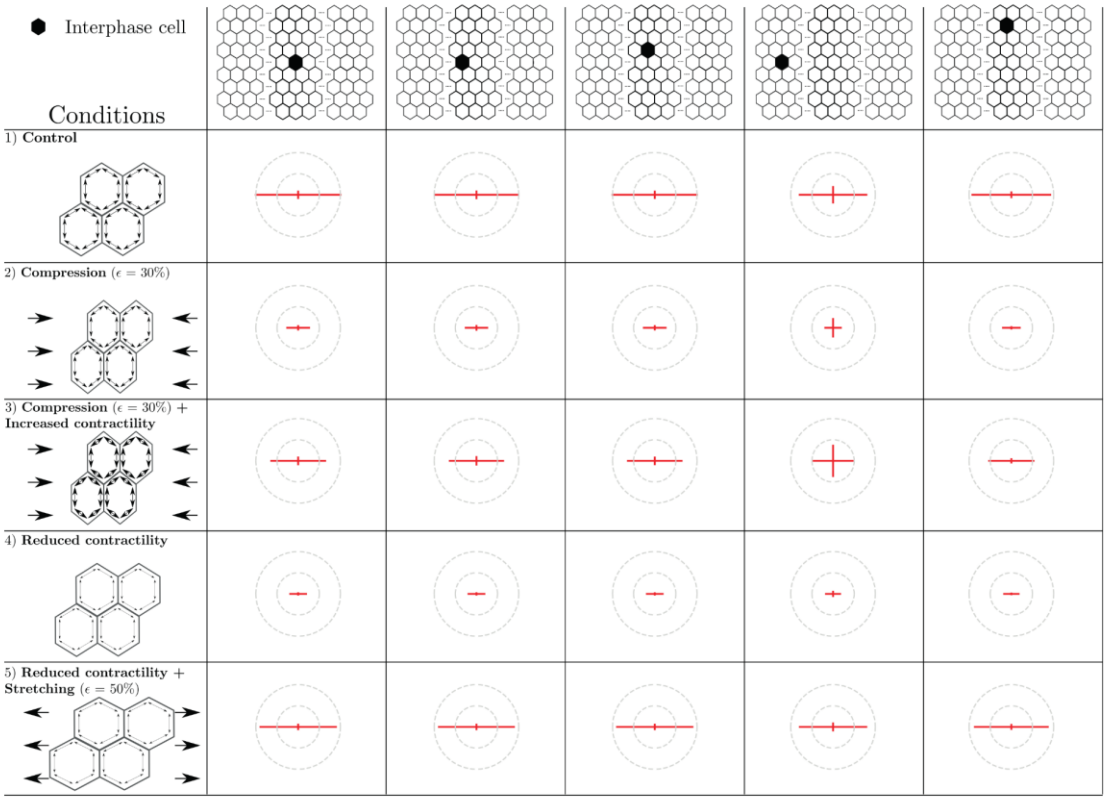

Figure S12. Principal stresses in cells within monolayers consisting entirely of interphase cells. Principal stresses are represented by orthogonal line segments with a length equal to the stress amplitude and a colour encoding their sign (red for tensile stress and blue for compressive stress). The stress tensor is plotted for different cell locations (each corresponding to a column): a cell at the centre of the monolayer, a cell directly adjacent to the central cell, a cell directly above the central cell, a cell far from the central along the x-axis, and a cell far above the central cell on the y-axis. Each row depicts a different experimental condition: untreated monolayer, compressed monolayer, compressed monolayer with increased contractility (via calyculin treatment), unloaded monolayer with reduced contractility (via Y27632 treatment), stretched monolayer with reduced contractility. Stress tensors are normalised to the stress tensor in control conditions (0% strain).

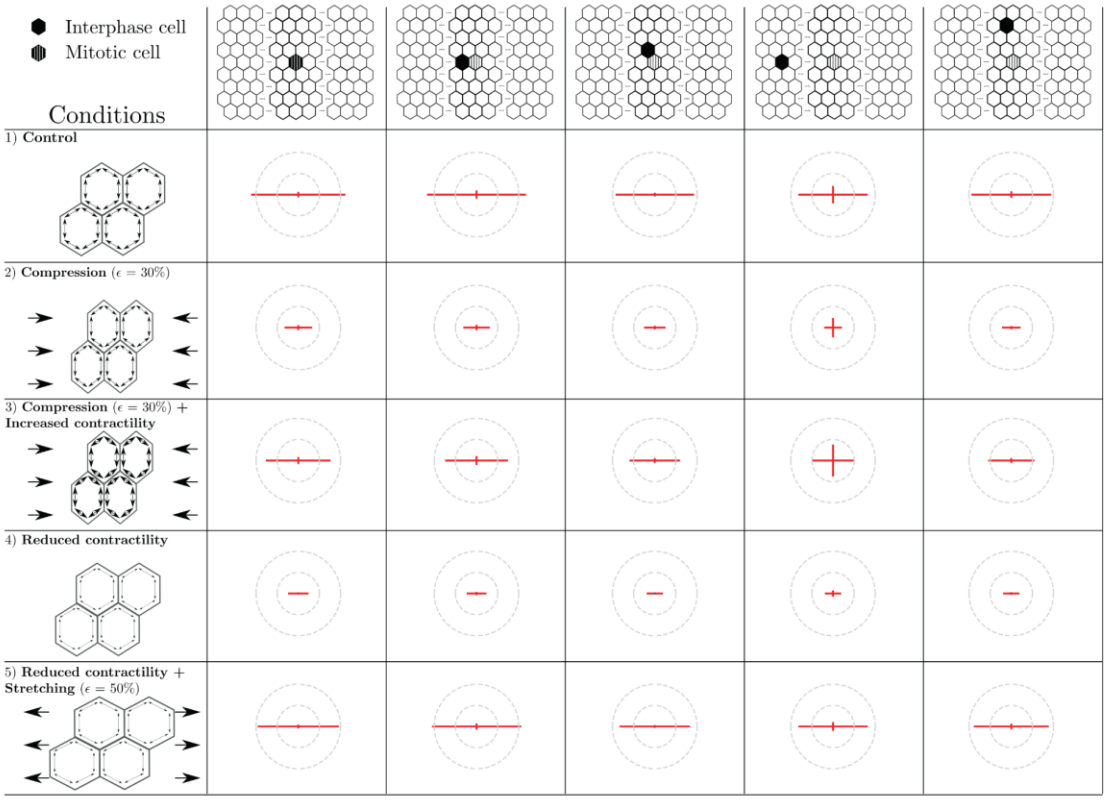

Figure S13. Principal stresses in cells within monolayers consisting of interphase cells with a mitotic cell in their centre. The mitotic cell is represented by the hashed hexagon. Principal stresses are represented by orthogonal line segments with a length equal to stress amplitude and a colour encoding their sign (red for tensile stress and blue for compressive stress). The stress tensor is plotted for different cell locations (each corresponding to a column): the mitotic cell in the centre of the monolayer, an interphase cell directly adjacent to the mitotic cell, an interphase cell directly above the mitotic cell, an interphase cell far from the mitotic cell along the x-axis, and an interphase cell far above the mitotic cell on the y-axis. Each row depicts a different experimental condition: untreated monolayer, compressed monolayer, compressed monolayer with increased contractility (via calyculin treatment), unloaded monolayer with reduced contractility (via Y27632 treatment), stretched monolayer with reduced contractility. Stress tensors are normalised to the stress tensor in control conditions in the centre of the monolayer without inclusion (**Fig S12**, first row, first column).

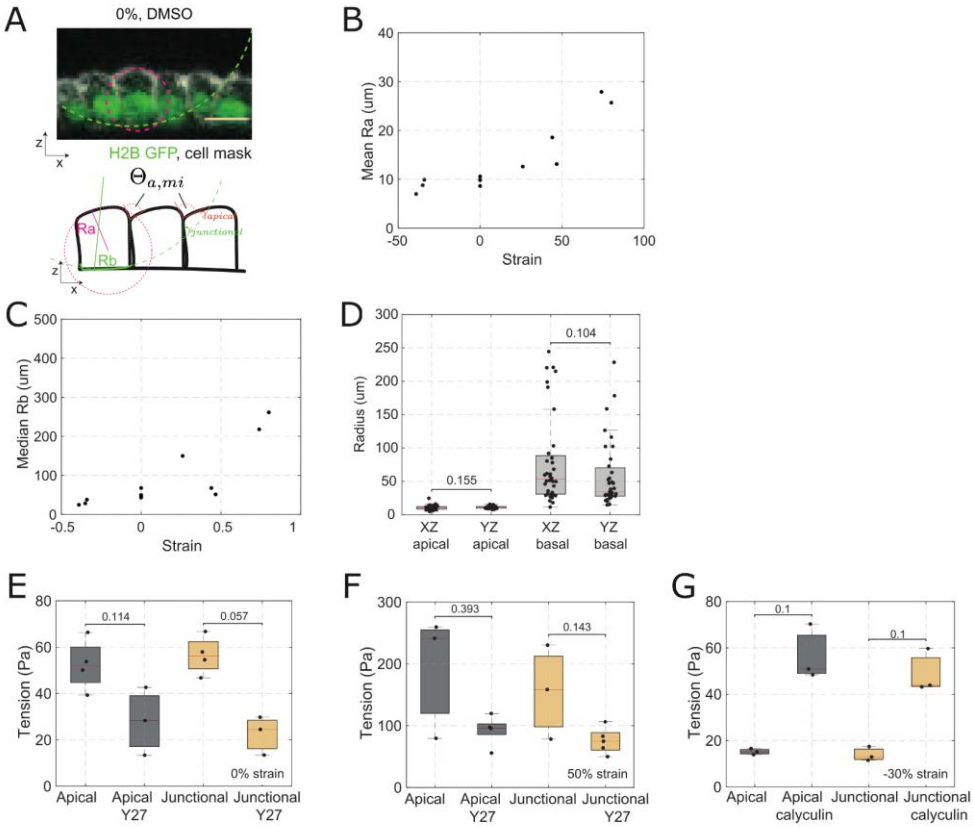

Figure S14. The apical and basal radii of curvature increase non-linearly with strain.

- **A.** Top: Representative profile of interphase cells within a monolayer at 0% strain, treated with DMSO. The basal and apical radii of curvature are indicated by a green dashed line and a magenta dashed line, respectively. Nucleic acids are visualised by H2B GFP (green), the cell membrane is labelled with CellMask 568 dye (white). Bottom: Diagram of the profile of interphase cells indicating the apical contact angles, θ_a, the tension at the intercellular junctions $\gamma_{junctional}$ and the tension at apical junctions γ_{apical} (**see methods**).
- **B.** Mean apical interphase radius as a function of strain. Each data point represents the average apical radius from a minimum of 20 interphase cells in a monolayer. Values for three monolayers are given for each strain range.
- **C.** Median basal interphase radius as a function of strain. Each data point represents the median basal radius from a minimum of 20 interphase cells in a monolayer. Values for three monolayers are given for each strain range.
- **D.** Apical and basal radii measured in the XZ and YZ direction. Each data point represents one cell. A minimum of 10 cells per monolayer from 3 different monolayers at 0% strain were measured. Box plots indicate the 25th and 75th percentiles, the red line indicates the median, and the whiskers extend to the most extreme data points that are not outliers. Individual data points are indicated by black dots. No significant differences were detected between radii measured in the XZ and YZ directions. XZ vs. YZ apical: p=0.155 (WRST); XZ vs. YZ basal: p=0.104 (WRST).
- **E.** Absolute surface tension of apical and junctional surfaces for control and Y27632-treated monolayers at 0% strain (as in Fig 5F).
- **F.** Absolute surface tension for apical and junctional surfaces for control and Y27632-treated monolayers at 50% strain (as in Fig 5F).
- **G.** Absolute surface tension for apical and junctional surfaces for control and calyculin-treated monolayers at -30% compressive strain (as in Fig 5F).

Supplementary tables

Strain (in %)	**-30%**	**0%**	**30%**	**50%**
Average (Z_ana-Z_meta)	-2.16	-2.30	-3.07	-5.41
Median (Z_ana-Z_meta)	-1.4	-1.5	-1.5	-4.7
Z-test compared to 0	0.97	0.99	0.96	0.9998
Number of divisions	145	79	27	66

Supplementary Table 1: The mitotic spindle does not rotate along the z-axis between the start of metaphase and the end of anaphase. All angles were measured in degrees. The Z-angle was measured at the beginning of metaphase (Z_meta) and at the end of anaphase (Z_ana). Data from at least 3 independent days for each condition.